



**HAL**  
open science

## Fluid-induced earthquakes with variable stress drop

Olivier Lengliné, L. Lamourette, L. Vivin, Nicolas Cuenot, Jean Schmittbuhl

► **To cite this version:**

Olivier Lengliné, L. Lamourette, L. Vivin, Nicolas Cuenot, Jean Schmittbuhl. Fluid-induced earthquakes with variable stress drop. *Journal of Geophysical Research*, 2014, 119 (12), pp.10.1002/2014JB011282. 10.1002/2014JB011282 . hal-01111195

**HAL Id: hal-01111195**

**<https://hal.science/hal-01111195>**

Submitted on 12 Oct 2021

**HAL** is a multi-disciplinary open access archive for the deposit and dissemination of scientific research documents, whether they are published or not. The documents may come from teaching and research institutions in France or abroad, or from public or private research centers.

L'archive ouverte pluridisciplinaire **HAL**, est destinée au dépôt et à la diffusion de documents scientifiques de niveau recherche, publiés ou non, émanant des établissements d'enseignement et de recherche français ou étrangers, des laboratoires publics ou privés.

Copyright

## RESEARCH ARTICLE

10.1002/2014JB011282

## Key Points:

- We observe repeating events in a geothermal reservoir
- These events show strong variation of seismic stress drop
- We relate these stress drop variations to change of normal stress

## Correspondence to:

O. Lengliné,  
lengline@unistra.fr

## Citation:

Lengliné, O., L. Lamourette, L. Vivin, N. Cuenot, and J. Schmittbuhl (2014), Fluid-induced earthquakes with variable stress drop, *J. Geophys. Res. Solid Earth*, 119, 8900–8913, doi:10.1002/2014JB011282.

Received 13 MAY 2014

Accepted 5 NOV 2014

Accepted article online 10 NOV 2014

Published online 4 DEC 2014

## Fluid-induced earthquakes with variable stress drop

O. Lengliné<sup>1</sup>, L. Lamourette<sup>1</sup>, L. Vivin<sup>1</sup>, N. Cuenot<sup>2</sup>, and J. Schmittbuhl<sup>1</sup>

<sup>1</sup>EOST, IPGS, CNRS, Université de Strasbourg Strasbourg, France, <sup>2</sup>GEIE Exploitation Minière de la Chaleur, Kutzenhausen, France

**Abstract** The static stress drop of an earthquake, which quantifies the ratio of seismic slip to the size of the rupture, is almost constant over several orders of magnitudes. Although variations are often observed, it is difficult, however, to attribute these variations either to a well-defined phenomenon or simply to measurement uncertainty. In this study we analyze the static stress drop of earthquakes that occurred during a water circulation test in the Soultz-sous-Forêts, France, geothermal reservoir in 2010. During this circulation test, 411 earthquakes were recorded, the largest event having a magnitude  $M_D 2.3$ . We show that several earthquakes in the reservoir can be combined into groups of closely located similar repeating waveforms. We infer that the amplitudes, and hence magnitudes, vary between the repeaters although the waveforms and spectra are both similar in shape. We measure similar corner frequencies for these events despite their different magnitudes, suggesting a similar rupture size. Our results imply that events at the same location may exhibit stress drop variations by as much as a factor of 300. We interpret that this variation in stress drop is caused by fluid pressure at the interface reducing the normal stress. We also hypothesize that the observed variations reflect a transition from stable to unstable slip on the imaged asperities.

## 1. Introduction

The deformation of the Earth's crust occurs over a very broad range of time and length scales. This is expressed by the diversity of phenomena and recorded signals, from continuous creeping and slow slip events captured by geodetic instruments to dynamic earthquake ruptures [e.g., Peng and Gomberg, 2010; Meng et al., 2011]. Despite their distinct expressions, all these modes of failure represent shear slip episodes on a localized interface [e.g., Brown et al., 2009; Latour et al., 2011]. However, determining the exact mode of failure that will occur on a given interface remains challenging. This is notably because temperature [Wiens, 2001], pore fluid pressure and related normal stress variations [e.g., Lockner et al., 1982; Ito and Obara, 2006; Brodsky and Mori, 2007; Ougier-Simonin and Zhu, 2013], material property changes [e.g., Kaneko et al., 2011], and the topography of the interface [Candela et al., 2011; Harrington and Brodsky, 2009] have all been shown to influence the rupture behavior.

Knowing the exact values of these different properties locally on the fault plane is currently very challenging. Furthermore, it also remains difficult to identify the scale at which each of these parameters influences the rupture style and to link an observed phenomenon to a well-identified parameter [e.g., Ben-Zion, 2008]. It thus remains challenging to resolve the factors controlling the earthquake rupture style and the broad spectrum of fault surface displacement recorded on the Earth surface.

When the analysis of slip behavior is restricted to the special case of dynamic ruptures, the failure mode has been shown to be linked to scaling laws relating the different earthquake source parameters [e.g., Kanamori and Brodsky, 2004]. However, even if scaling laws are observed for most earthquakes, deviations are also observed [e.g., Kanamori, 2004; Allmann and Shearer, 2009; Duputel et al., 2013; Baltay et al., 2011]. Capturing the influence of the local environmental conditions on these deviations remains difficult, as the physical properties of the fault surface are generally not precisely known. Hence, we are restricted to comparing earthquakes from different locations for which only some broadscale information about the fault surface is known.

At an intermediate length scale between the fault zone and the laboratory, geothermal reservoirs are a natural system for which some parameters can be tuned in a somewhat controlled way. It thus offers the possibility to test the influence of environmental conditions on the earthquake source properties at a given location and thus overcome most of the limitations exposed previously. To ensure that we are isolating

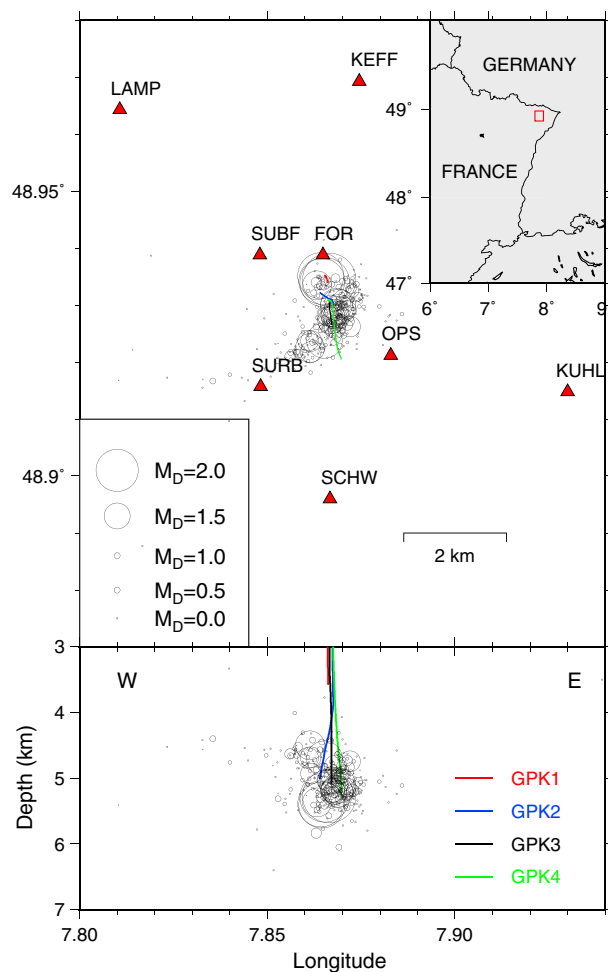


**Figure 1.** (top) Localization of the 393 located events (circles). The circle radius is related to the magnitude of the events. The seismic station sites are indicated by red triangles. The color lines show the trajectories of the geothermal wells. The enclosed map shows the location of the geothermal area. (bottom) Cross section showing the depth distribution of the earthquakes as a function of the longitude. We observe a clustering of the events with depth close to the injection point.

very similar waveforms (multiplets) and focus our analysis on four of these clusters. The relative relocations of the events in these four groups indicate that they are rupturing the same fault patch of the fault plane. However, and despite the waveform and location similarity, these events have different amplitudes and hence different magnitudes. By employing a spectra ratio technique, we show that all the earthquakes within a group have similar corner frequencies and hence durations, yet varying magnitudes.

We are able to resolve relative stress drop variations between collocated events. Namely, we show that some events show a very low stress drop of the order of tens of kilopascals. As the local fluid pressure may vary during the circulation experiment, static stress drop variations are interpreted as a change in the effective normal stress at the location of the seismic asperity. It also suggests that by reducing the effective normal stress on the interface, a larger fraction of the fault plane displacement occurs aseismically. Therefore, we show that, the same interface may have a different behavior depending on the environmental condition, and we discuss how normal stress can influence the earthquake rupture behavior.

## 2. Data

The Soutz-sous-Forêts geothermal power plant is located in the northeastern part of France, close to the border with Germany, in the Upper Rhine Graben (Figure 1). The local geological structure of the Soutz

source properties, the use of repeating earthquakes guarantees that we are always observing the same fault area, influenced by the same local conditions.

In the present study, we analyze the control on seismic slip,  $D$ , during an earthquake, and in particular, deviations from the aforementioned scaling laws, i.e., relating seismic slip to earthquake source dimension,  $r$ .

The static stress drop,  $\Delta\sigma$ , is defined for a circular rupture as

$$\Delta\sigma = \frac{7\pi}{16} \mu \frac{D}{r}, \quad (1)$$

where  $\mu$  is the shear modulus of the host rock [Eshelby, 1957]. As such, it is a direct measure of the scaling between slip,  $D$ , and the source dimension,  $r$ . In the above equation, and throughout this manuscript, the quantities  $D$  and  $\Delta\sigma$  should be interpreted as averaged values over the whole ruptured area.  $\Delta\sigma$  has been observed to vary in a limited range, typically [0.1–10] MPa for earthquakes over a large range of magnitude [e.g., Kanamori and Brodsky, 2004]. Here we test how the variation in normal stress caused by fluid injection in the geothermal reservoir might affect the static stress drop of the recorded events.

We first analyze all the earthquakes detected during a 1 yearlong circulation test performed at the Soutz-sous-Forêts geothermal reservoir during the year 2010. Among the recorded earthquakes we then identify groups of events with

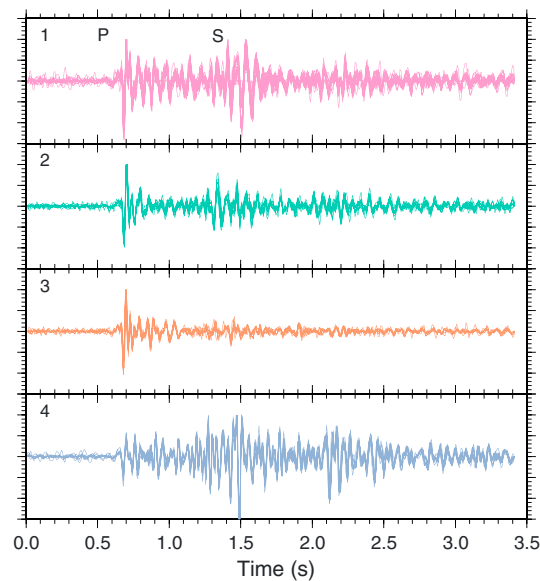


**Figure 2.** Waveforms recorded on the vertical component sensor at various station sites for the four selected multiplets. Waveform of each event is normalized by its maximum amplitude. For each multiplet, the waveforms of all events are represented by the same color and are superimposed. All waveforms have been aligned on the *P* wave arrival and are filtered in the range 10–40 Hz. We notice the high similarity of the waveforms for more than 3 s and for all groups. Groups are identified by the number in the upper left corner.

times of the entire earthquake sequence in order to obtain the most reliable estimations of the arrival times of the earthquakes at the maximum number of stations. Events without a sufficient number of clear arrivals were rejected at this stage. Following this procedure, we kept 393 events out of the initial number of 411. The location of each event was determined with the Hypoinverse-2000 software [Klein, 2002] using a 1-D velocity model derived for the Soultz area: we take the *P* wave velocity in the granite at 5 km depth to be 5.9 km s<sup>-1</sup> [Cuenot et al., 2008]. Our locations are in good agreement with those obtained from the automatic procedure and all earthquakes locate within a few kilometers of the injection point and close to the injection depth of 5 km in the geothermal reservoir (Figure 1).

### 3. Similar Events

We look for the presence of repeating earthquakes in order to identify possible ruptures of the same fault patch. For all possible pairs of earthquakes we first compute the spectral coherency between earthquake traces. Coherency,  $C(f)$ , is computed from a 256 sample long window (1.7 s) starting 0.3 s before the *P* wave arrival. For most stations, our window thus includes both the *P* and the *S* wave arrivals. We only use the vertical component seismograms, as horizontal components are not available at all stations. Notating  $X(f)$  and  $Y(f)$  the spectrum of the signals  $x(t)$  and  $y(t)$  from the two earthquakes considered,  $C(f)$  is obtained through

$$C(f) = \frac{\overline{X(f)Y^*(f)}}{\sqrt{\overline{X(f)X^*(f)}}\sqrt{\overline{Y(f)Y^*(f)}}}, \quad (2)$$

where  $f$  is the frequency, the asterisk denotes the complex conjugate and the overbar indicates smoothed values by the Fourier Transform of a Hann window of order 4. A mean coherency is obtained by averaging the value of  $C(f)$  in the frequency range [10–40] Hz. We tested several frequency bands in order to best discriminate similar events among the overall seismicity and found that this range is the most suited to resolve the similarity between events. We discuss at the beginning of section 7 the possible effects of the limited data bandwidth on our results. If the mean coherency is higher than 0.9 at least at two stations, then the two earthquakes are linked and are considered part of the same multiplet. Among the 393 events, 79 repeaters

region corresponds to a 1400 m thick sedimentary cover overlaying a crystalline basement made of altered and fractured granitic rocks [Hooijkaas et al., 2006]. The geothermal reservoir has undergone several stimulation and circulation periods since the start of the geothermal project in 1987. During these tests, water was injected in one or several wells as deep as 5 km, and abundant microseismicity was observed [e.g., Charléty et al., 2007; Cuenot et al., 2008; Dorbath et al., 2009]. The 2010 circulation test began in November 2009 and lasted 11 months, and the related seismicity was monitored by a dedicated local network consisting of eight seismic stations located at the surface and within 6 km of the injection site. All seismic sites have vertical sensors recording at a sampling frequency of 150 Hz, and three stations also have horizontal sensors. An automatic procedure dedicated to the routine monitoring of the geothermal reservoir detected 411 seismic events over the course of this 2010 circulation, and duration magnitudes assigned to the events range from  $M_D$  -0.3 to 2.3. Six earthquakes were of magnitude 1.8 or larger and four of them were magnitude 2.0 or larger [Cuenot et al., 2011]. Based on the detection times, we review manually all *P* and *S* picking

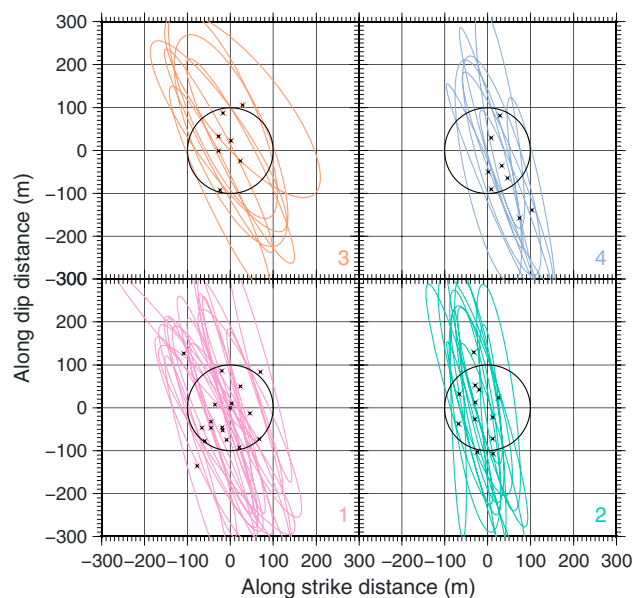


**Figure 3.** Relocalization of events in a same multiplet. Each subfigure represents the relative relocation of events for each group. The 95% confidence area of the relocated events is indicated by the ellipses. Crosses indicate the center of the ellipses for each event. One event from group 2 and from group 3 were removed as they do not locate close enough to the other events of the multiplet. Results are projected along the inferred fracture orientation in this part of the reservoir, a dip of  $71^\circ$  and a dip direction of  $234^\circ$  [Sausse *et al.*, 2010]. The circle represents for reference the rupture size of an event with a 100 m radius.

a given group are within tens of meters to a few hundreds of meters of each other (Figure 3). We compute uncertainties associated with the relocation procedure following the method of Got *et al.* [2011] but find that even when considering the uncertainties, the events are still very closely located, suggesting that these events can be considered repeaters.

Because of the limited resolution of our relocation in the dip direction, and to check that repeating events corresponds to events sharing the same source area, we compute the difference of the *S*-minus-*P* traveltimes for events in each group. This is achieved by running a correlation between the two signals of a given pair at the times of the *P* wave and the *S* wave arrivals and subtracting the two inferred delays. The cross-correlation function is interpolated in the time domain in order to achieve a subsample estimation of the time delays. For all groups we find that the maximum *S*-minus-*P* traveltime difference is always lower than 1 sample, except for the first group where a delay of 1.5 samples was observed. These *S*-minus-*P* traveltime differences correspond to distance variation in the ray direction of the order of 22 m and 33 m, respectively. We will show in section (5) that these distances are much smaller than the inferred source dimensions suggesting that the events of the same group share the same rupture area.

#### 4. Relative Moments

Despite sharing a similar waveform shape and an almost equivalent location, individual events in each multiplet display large amplitude variations. This is clearly visible in Figure 4 where we show the waveforms, recorded at the same station, of two events of the same group (group 4) which present the largest variation of amplitude (the magnitude of the two events is  $M_D = 0.1$  and  $1.8$ ). We notice that these two events have a very similar waveform shape which is expected as this similarity is a selection criterion for events being considered as part of the same group. We can roughly estimate a factor of 200 of relative amplitude difference between these two events at the station shown in Figure 4 by comparing the peak amplitudes reached by these two events. In order to get the most reliable estimates of the relative amplitude variations between events of the same group we employed a singular value decomposition (SVD) approach. This approach

separate into seven groups each with nine or more events. We focus our study on four groups of multiplets which have at least one earthquake with magnitude  $M_D > 1$  (Figure 2). These four groups contain 19, 13, 9, and 9 events, respectively. Interestingly we note that four out of the largest six events recorded during the circulation experiment are included in the selected groups.

In order to discard outliers and ensure that all events are located on similar fault patches, we relocate the considered earthquakes using double-difference relocation, following the procedure of Got *et al.* [1994] and Got and Okubo [2003]. We project all relocation results into the most likely fracture plane inferred for the Soultz-sous-Forêts reservoir. This fracture, the largest of the reservoir, has a dip of  $71^\circ$  and a dip direction of  $234^\circ$  [Sausse *et al.*, 2010], and its location is consistent with the position of the earthquakes analyzed in this study. Our relocation results highlight that almost all of the earthquakes of

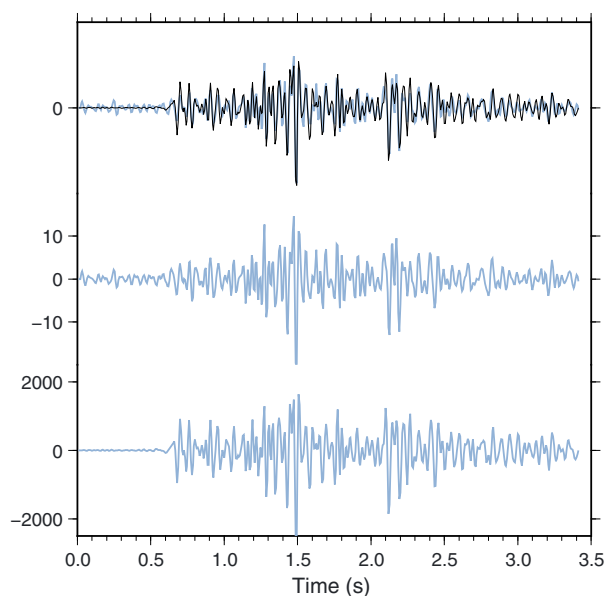


**Figure 4.** Seismograms recorded at the same station (KEFF) for the two events of group 4 with the largest and lowest amplitude ( $M_D$  1.8 and  $M_D$  0.1 events). The epicentral source-site distance is 4.4 km, and the two events are located less than 80 m apart. The top figure shows the events with normalized amplitudes and we see the extreme similarity between the two events. The two seismograms below are the two same events but with their original amplitude. We notice that despite the similarity of the waveforms, we observe a large variation of amplitude between the two signals.

has proved to produce precise estimates of these values when dealing with similar events as in our case [Rubinstein and Ellsworth, 2010]. The method relies on the comparison of the amplitude of the first output basis vector that results from the singular value decomposition. This first vector will represent the part of the signal common to all events of the sequence and thus provides a measurement less affected by noise. For each of the four sequences, and at each station, we first aligned the waveforms of all the events of the group and performed the SVD. At each station, we take the amplitude of the first basis vector to be the amplitude of that event and then average the amplitude for each event over all stations and normalized by the largest event in each multiplet. We resolve for each group, amplitude variations as large as a factor 61, 314, 91, and 256 for groups 1 to 4, respectively (Table 1). This variation reflects the large difference in the waveform amplitudes that can exist from earthquakes with similar waveforms and can be directly related to a variation of moment,  $M_0$ . This implies that the events of the same group can show a factor up

to nearly 300 in moment variation. This estimation is compatible with the difference inferred from the catalog magnitude of the events. Following [Kanamori, 1977], we can roughly estimate that a factor  $\sim 300$  in moment variation implies a factor of  $\log_{10}(300)/1.5 \approx 1.7$  in moment magnitude between the two events, similar to the catalog  $M_D$  from these events, which range from  $M_D$  0.0 to  $M_D$  2.1.

### 5. Estimating Sources Dimension

We consider whether different events of a given multiplet, despite very similar waveforms, show variations in rupture area, by estimating relative difference in rupture dimension,  $r$ . We first compute the rupture size for the largest event of each group. To do so, we deconvolve the original signal from instrumental response and convert it to displacement. Displacement spectra are then computed from a 128 sample long window encompassing the  $P$  wave arrival. We average all spectra obtained at the different stations to cancel out possible directivity effects and minimize the site effect at each station. We finally obtain a displacement spectrum for each event. Fitting the omega square model of [Brune, 1970], we estimate a corner frequency,  $f_c$ , for these events although uncertainties are quite large (Figure 5). For the four events, the largest in each group, we find that  $f_c$  is in the range [10–20] Hz. The corner frequency might be larger for the event of group 1 which has the smallest magnitude, but it could still be within the inferred range given the uncertainties of the estimation. Interpreting this result in terms of a rupture radius, we arrive at

$$r = \frac{k\beta}{f_c} \tag{3}$$

where  $k = 0.32$  for  $P$  wave [Madariaga, 1977] and  $\beta = 3371 \text{ m s}^{-1}$  [Cuenot et al., 2008] is the shear wave speed. It leads to an estimate of  $r = 54\text{--}108 \text{ m}$  given the bounds on the estimation of  $f_c$ . Such rupture dimension is typical for earthquakes of the same magnitude as those analyzed ( $M_D = 1.4\text{--}2.1$ ) assuming a typical stress drop of 3 MPa [e.g., Abercrombie, 1995; Kanamori and Brodsky, 2004].

We now estimate the relative difference of corner frequency between all events in the same multiplet. We employ a spectral ratio approach to recover the variation in corner frequency for all pairs of events in

**Table 1.** Results Detailing Relative Stress Drop Obtained for Each Event in the Four Groups<sup>a</sup>

Group Number	Event Number	Time (days)	$r$ (m)	$M_0^r$	$\Delta\sigma_0^*/\Delta\sigma^*$	$\Delta\sigma_0/\Delta\sigma$	$M_D$
1	1	103.632	79.087	0.08877	10.49	11.26	0.1
1	2	104.645	82.575	0.04260	24.87	23.48	0.1
1	3	104.658	78.471	0.12068	7.53	8.29	0.3
1	4	119.941	80.943	0.81452	1.23	1.23	1.4
1	5	150.645	70.249	0.06200	10.52	16.13	0.1
1	6	232.357	87.076	0.57230	2.17	1.75	1.4
1	7	232.418	77.340	0.44554	1.95	2.24	1.1
<b>1</b>	<b>8</b>	<b>232.424</b>	<b>81.000</b>	<b>1.00000</b>	<b>1.00</b>	<b>1.00</b>	<b>1.4</b>
1	9	232.769	86.195	0.17516	6.88	5.71	0.7
1	10	249.038	72.667	0.04617	15.64	21.66	0.3
1	11	264.209	80.597	1.47673	0.67	0.68	0.5
1	12	284.419	84.918	0.05722	20.14	17.48	-0.3
1	13	286.788	90.536	0.02416	57.80	41.39	0.1
1	14	287.237	89.935	0.04139	33.07	24.16	0.1
1	15	342.414	76.267	0.10579	7.89	9.45	0.1
1	16	342.613	81.178	0.20560	4.90	4.86	0.1
1	17	342.690	73.643	0.33161	2.27	3.02	0.2
1	18	342.792	82.762	0.24993	4.27	4.00	0.6
1	19	342.794	75.969	0.21196	3.89	4.72	0.6
2	1	110.160	73.818	0.00899	84.16	111.19	0.3
2	2	110.787	70.520	0.02323	28.40	43.04	0.5
2	3	113.963	72.281	0.00534	132.96	187.11	0.1
2	4	115.645	76.356	0.01258	66.61	79.52	0.0
2	5	115.647	67.804	0.01767	33.20	56.60	0.1
2	6	115.688	78.266	0.06328	14.26	15.80	0.5
<b>2</b>	<b>7</b>	<b>117.013</b>	<b>81.000</b>	<b>1.00000</b>	<b>1.00</b>	<b>1.00</b>	<b>2.1</b>
2	8	117.192	73.852	0.02549	29.73	39.22	0.5
2	9	125.442	72.791	0.04647	15.62	21.52	0.7
2	10	131.339	69.529	0.02497	25.33	40.05	0.3
2	11	132.079	67.682	0.00318	183.54	314.61	0.0
2	12	156.584	77.234	0.01177	73.65	84.95	-0.3
3	1	95.053	84.550	0.19190	5.93	5.21	0.8
3	2	95.434	70.176	0.22087	2.94	4.53	0.7
<b>3</b>	<b>3</b>	<b>95.488</b>	<b>81.000</b>	<b>1.00000</b>	<b>1.00</b>	<b>1.00</b>	<b>1.8</b>
3	4	95.713	59.033	0.07333	5.28	13.64	0.5
3	5	96.102	61.227	0.01089	39.66	91.83	0.3
3	6	96.510	65.642	0.02523	21.09	39.63	0.2
3	7	144.821	63.502	0.01338	36.01	74.73	0.1
3	8	144.822	59.480	0.07995	4.95	12.51	0.4
4	1	140.129	68.379	0.02114	28.46	47.31	0.7
4	2	179.522	85.454	0.06787	17.30	14.74	0.3
4	3	184.114	69.605	0.01496	42.41	66.84	0.1
4	4	190.915	80.067	0.14239	6.78	7.02	1.7
4	5	198.623	73.593	0.01488	50.41	67.22	0.1
4	6	199.519	74.683	0.02654	29.53	37.67	0.3
<b>4</b>	<b>7</b>	<b>205.517</b>	<b>81.000</b>	<b>1.00000</b>	<b>1.00</b>	<b>1.00</b>	<b>1.8</b>
4	8	214.114	66.810	0.01549	36.24	64.58	0.3
4	9	268.088	78.101	0.00389	230.24	256.84	0.1

<sup>a</sup>Time is given in days since the start of the circulation experiment (1 November 2009). The rupture dimension  $r$  is estimated assuming the largest magnitude event in each group has a radius of  $r=81$  m (the average of 54 and 108 m). Relative moment are given by  $M_0^r$ . The first variation of stress drop  $\Delta\sigma_0^*/\Delta\sigma^*$  is estimated taking into account the relative size variation between events. The second variation of stress drop  $\Delta\sigma_0/\Delta\sigma$  is obtained assuming that all events of a same group have the same rupture size. All stress drop variations are normalized by the stress drop of the largest event of the group ( $\Delta\sigma_0$  or  $\Delta\sigma_0^*$ ). The last column gives the catalog magnitude. The reference event of each group is shown in bold face.

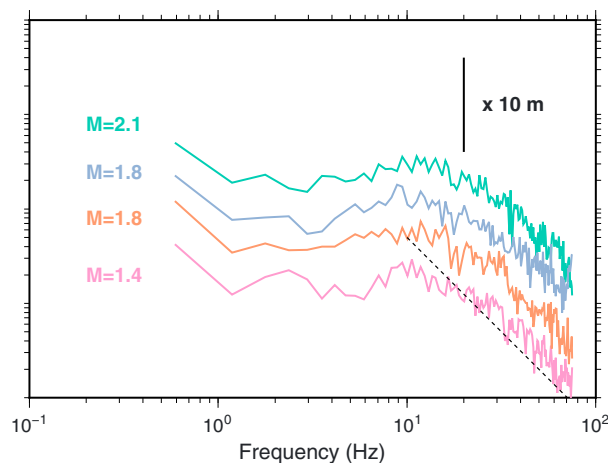


**Figure 5.** Displacement Fourier spectra computed on the *P* wave for the largest magnitude event of each group. Spectra have been shifted vertically to enhance visibility. Spectra are obtained after deconvolving the signal from the instrument response and converting velocity into displacement. We then average the spectra computed at all station in order to cancel as much as possible path and site effects to get a spectrum for each event. The magnitude of the events is indicated on the left and the dashed line represents a  $f^{-2}$  decay.

estimated as the modulus of the transfer function relating the Fourier transform of the processed pair of events as performed in *Got and Fréchet [1993]* and *Lenliné and Got [2011]*. Namely, we take

$$G(f) = \frac{X(f)Y^*(f)}{Y(f)X^*(f)}, \tag{4}$$

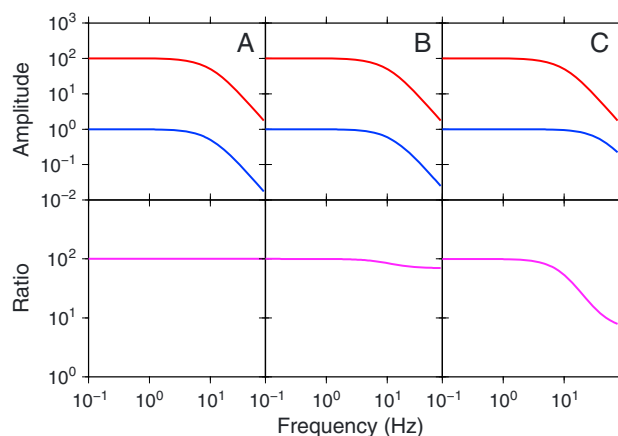


**Figure 6.** Scheme depicting three different cases of earthquake pairs. For each case we represent the *P* wave displacement spectra of the (top) two events and (bottom) their spectra ratio. (a) The two earthquakes have the same corner frequency but different amplitudes. The spectral ratio is flat over the entire frequency range. (b) The two earthquakes have almost the same corner frequency and different amplitudes. The spectral ratio can be well fitted by a linear function around the corner frequency of the two events. (c) In the third scenario, the two earthquakes have two different amplitudes and different corner frequencies. In this case the spectral ratio is not flat anymore and we expect a transition between the corner frequencies of the two events.

the same sequence. For closely located earthquakes, spectral ratio for records at the same station will cancel all propagation and station terms, leaving only source information of the two events. The spectral ratio method has been traditionally used to recover source properties of a larger event using a smaller colocated event as an empirical Green function [e.g., *Hough, 1997; Mayeda and Walter, 1996; Mayeda et al., 2007; Malagnini et al., 2010; Baltay et al., 2010, 2011; Kane et al., 2011*].

Here, however, we compare the spectra of all possible event pairs within a multiplet, regardless of their relative magnitude differences, to determine the relative source parameters. This method is expected to yield much more precise results of the variation of earthquake source sizes than a direct comparison of the corner frequency from the displacement spectra. The spectral ratio,  $G(f)$ , is

where  $X(f)$  and  $Y(f)$  are estimated on a 128 sample long window around the *P* wave arrival and spectral densities are smoothed by the Fourier transform of a Hann window of order 4. We assume a circular crack model for the two earthquakes in the pair. Following *Brune [1970]* and *Madariaga [1977]*, the far-field displacement source spectrum,  $X(f)$ , decays after the corner frequency,  $f_c$ , as  $X(f) \propto f^{-2}$ . Denoting  $f_{c1}$  and  $f_{c2}$  as the corner frequency of the first and second earthquake in the pair, respectively, it yields

$$\ln[G(f)] = \alpha + \ln \left[ \frac{1 + \left(\frac{f}{f_{c2}}\right)^2}{1 + \left(\frac{f}{f_{c1}}\right)^2} \right] \tag{5}$$

where  $\alpha$  denotes the ratio of the low-frequency spectral level. Assuming that  $f_{c1} < f_{c2}$ , the spectral ratio is flat at frequencies lower than  $f_{c1}$  and greater than  $f_{c2}$  and transitions from one level to the other in the interval  $[f_{c1}, f_{c2}]$ . We can therefore obtain the corner frequencies



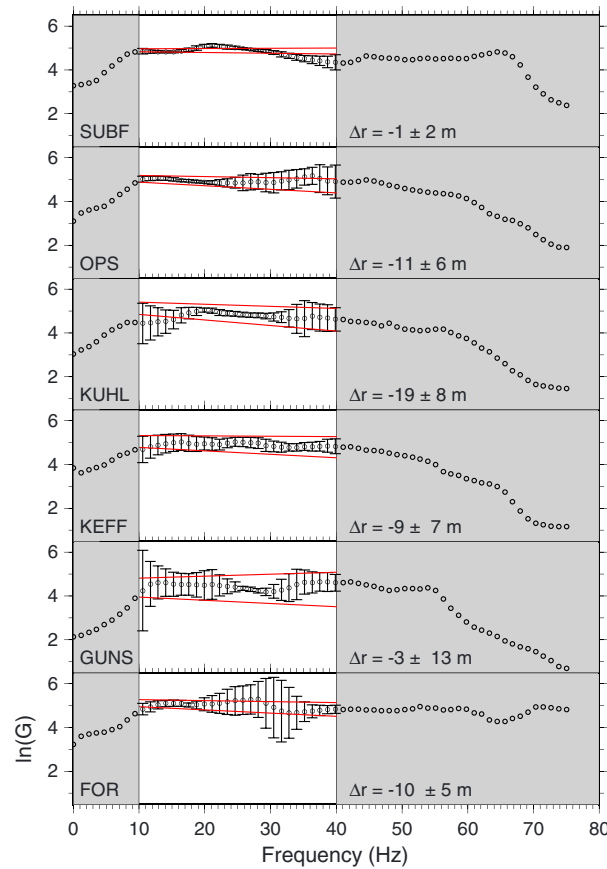


**Figure 7.** Circles represent logarithm of the spectral ratio between two events ( $M_D 1.8$  and  $M_D 0.1$ ) of the same group (group 4) computed at several stations using equation (4). Uncertainties of  $\ln[G(f)]$  are computed from the coherency values. The linear fit of  $\ln[G(f)]$  in the frequency range where we have similarity between the waveforms (10–40 Hz) is indicated by the two red lines. They represent the 95% confidence interval of possible fits. The associated variations of rupture dimension,  $\Delta r$  between the two events computed at each station is indicated.

extract a variation of rupture dimension between the two events as proposed by *Got and Fréchet* [1993]. Indeed, assuming  $f_{c1} \simeq f_{c2}$ , the corner frequency of the first and second event in the pair, we can approximate the slope of  $\ln[G(f)]$  to  $\Delta f_c / f_c^2$ , where  $\Delta f_c = f_{c1} - f_{c2}$ . Calling  $a$  the slope of  $\ln[G(f)]$ , i.e.,

$$a = \frac{d(\ln[G(f)])}{df} = 2f \frac{f_{c1}^2 - f_{c2}^2}{(f_{c2}^2 + f^2)(f_{c1}^2 + f^2)}. \quad (6)$$

Supposing that  $f_{c1} \simeq f_{c2} \simeq f_c$  we can pose  $f_{c1} = f_c + \epsilon_1$  and  $f_{c2} = f_c + \epsilon_2$  where  $\epsilon_1$  and  $\epsilon_2$  are small and can be positive or negative. Then from equation (6) it follows that the value of  $a$  in the vicinity of  $f_c$  is given by

$$a = 2f_c \frac{(f_{c1} - f_{c2})(2f_c + \epsilon_1 + \epsilon_2)}{(f_c^2 + 2\epsilon_2 f_c + f_c^2)(f_c^2 + 2\epsilon_1 f_c + f_c^2)} \quad (7)$$

$$a = \frac{4f_c^2(f_{c1} - f_{c2})}{4f_c^4} \left(1 + \frac{\epsilon_1}{2f_c} + \frac{\epsilon_2}{2f_c}\right) / \left(1 + \frac{\epsilon_1}{2f_c} + \frac{\epsilon_2}{2f_c}\right) \quad (8)$$

$$a = \frac{(f_{c1} - f_{c2})}{f_c^2} \quad (9)$$

of the two events in the pair by fitting the logarithm of the spectral ratios,  $\ln[G(f)]$ , to equation (5). We illustrate in the plots of Figure 6 the expected variation of the spectral ratio as a function of frequency for three different cases. Notably, we show the behaviors that one should observe when the two earthquakes in the pair have different corner frequencies as opposed to the case where the two corner frequencies are similar.

We compare these two cases with our data in Figure 7. Figure 7 shows the logarithm of the spectral ratio,  $\ln[G(f)]$ , computed at all available stations for the two events of group 4 that present the largest amplitude variation ( $M_D = 1.8$  and  $M_D = 0.1$ ). As expected due to the high similarity of the waveform, the spectral ratios are very flat and a clear transition of  $\ln[G(f)]$  which would have marked the corner frequencies of the two events in the range 10 to 40 Hz cannot be discerned. The almost flat spectral ratio is similar to the case reported in Figure 6 where the two events have a similar corner frequency. It thus suggests that the corner frequency of the two events is quite similar despite their very different amplitudes.

Because of these very similar corner frequencies, we search for small variations. Despite very similar corner frequencies, it is still possible to

when neglecting second-order terms. Following *Madariaga* [1977], we can relate the corner frequency of the event to the radius of the rupture size by using equation (3). Again supposing  $f_{c1} \simeq f_{c2}$ , it results that

$$\Delta f_c / f_c^2 = \frac{f_{c1} - f_{c2}}{f_c^2} \quad (10)$$

$$= \frac{\Delta r}{k\beta} \quad (11)$$

where  $\Delta r$  is  $r_2 - r_1$ . We note that in deriving equation (11), we hypothesize that all the variation in rupture duration are related to a change of the earthquake size. We discuss in section (7) the more general case where variations of rupture duration are not solely linked to a variation of rupture dimension. From equation (11) it follows that  $\Delta r = k\beta a$ . For each spectral ratio, and at each possible station we performed a linear fit on the value of  $\ln[G(f)]$  in the frequency range [10–40] Hz. This frequency range corresponds to the range where the coherency between events is the highest. It is also the expected range for the events corner frequencies given that we found an estimate of  $f_c$  between [10 and 20] Hz for the largest event of each group. However, even if the corner frequency of the events falls slightly outside the [10–40] Hz frequency range, the results obtained from equation (11) will still represent an acceptable approximation.

The slope of the best linear least square fit of  $\ln[G(f)]$  gives us an estimate of  $a$  that we translate into a variation of  $\Delta r$ . Measurements of  $\ln[G(f)]$  are assumed to be Gaussian with a standard deviation,  $\sigma(f)$ , estimated by  $\sigma(f) = (1 - C(f)^2)/C(f)^2$ . We also fix  $\sigma(f)$  to never be lower than 0.02, equivalent to  $C(f) > 0.99$ . As we are measuring the difference of rupture radius,  $\Delta r$  for all possible pairs and at all available stations, we can set a simple linear inverse problem to recover  $\Delta r$  for all events of the group relative to a common reference. We set the largest event of the group as the reference event and resolve the inverse problem as per *Lenliné and Got* [2011]. We finally determine the relative rupture radius for each event of the group. For example, we can see in Figure 7 that the difference in radius at all stations is at maximum of the order of tens of meters. The final estimate of  $\Delta r$  between these two events (the largest event and the smallest event), after combining all information of all possible pairs of earthquake gives  $\Delta r = 3 \pm 13$  m. For the four analyzed groups of similar earthquakes, we computed these estimates of relative rupture radius. We found that the average variation value of  $|\Delta r|$  computed over all possible pairs of events in a group are 5, 7, 13, and 7 m, respectively, for groups 1 to 4, respectively (Table 1). The uncertainties associated with these measurements are quite similar for each of the four sequences and are of the order of 10 m. It suggests that it is likely that all events of a given group have the same rupture dimension. Given our rupture dimensions found for the largest event of each group, our inferred measurements of  $\Delta r$  implies that the relative variation of rupture size is small compared to the rupture dimension. Even considering the case producing the largest relative variation of rupture dimension we obtained a factor of  $(54-13)/54 = 0.76$  of length variation, still close to 1.

In order to check the results of our spectral ratio approach, we want to identify if small earthquakes, occurring close to the multiplets but not included in it, present a distinct spectral shape. This would demonstrate our ability to distinguish earthquake source properties from their spectral content and validate the results obtained from the multiplets. Notably, it would show that by employing the spectral ratio approach, we are able to remove the attenuation effects that could mask the difference of corner frequency between two events. We identified two small earthquakes ( $M_D = 0$ ) close to the events of multiplet 4 (less than 100 m away from the multiplet barycenter). We show in Figure 8 the spectra of all earthquakes of group 4 recorded at a same station. We first notice the extreme similarity of the spectra for all these earthquakes that are part of the same group. This behavior is expected as earthquakes have been selected based on their high similarity in the spectral domain. We clearly observe a difference in frequency content for the two earthquakes not in the multiplet. Importantly, we notice a higher amplitude at high frequency for these two small earthquakes spectra. We also observe that the spectral ratio of these two events, with the largest event of group 4, show a much more pronounced decay in the investigated [10–40] Hz band, even at higher frequency. This behavior is more compatible with Figure 6c. It shows that we would have been able to distinguish a change of variation of corner frequency for events in the group if such variations were present.

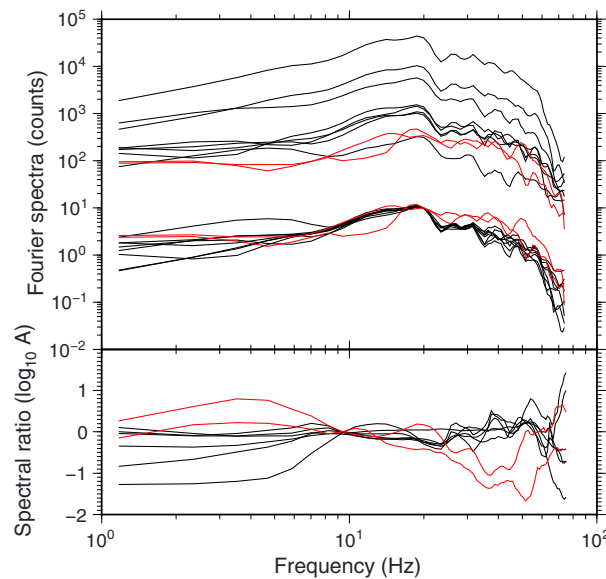


**Figure 8.** (top) Uncorrected velocity spectra computed directly from the recorded seismograms on a window around the *P* wave arrival. The black lines show the spectra estimated for each event of group 4 at the same station but for two small events close to the multiplet but which are not part of it. In the middle of the panel are the same spectra but normalized by their respective amplitude at 20 Hz. (bottom) Logarithm of the spectra ratio computed between the spectra represented in Figure 8 (top) and the spectrum of the largest event. All ratios are normalized by their amplitude at 10 Hz. We clearly observe a deviation from a constant ratio of the two events not included in the sequence. This deviation probably reflects a difference of corner frequency for these two events.

## 6. Variable Stress Drop Events

Given that we found source dimensions,  $r$ , to be similar for all events within a group, the areas,  $A$ , are also similar. We then obtain from

$$M_0 = \mu AD, \quad (12)$$

that the variation of seismic moment,  $M_0$ , can be interpreted as variation of seismic slip,  $D$ , by considering that the shear modulus at the location of the multiplet is constant. It results from equation (1) that the relative variation in the resolved seismic moment is directly reflecting a variation of seismic slip and seismic stress drop. It implies that we determine up to nearly a factor 300 of the seismic stress drop variation for events occurring at the same location.

Relaxing the hypothesis of a constant rupture area and taking the estimates of rupture sizes obtained from the spectral analysis, we can refine the estimates of stress drop variation while considering a constant shear modulus with time at the location of each multiplet. The estimates of stress drop variations between two events are then obtained from equations (1) and (12) as

$$\frac{\Delta\sigma_1}{\Delta\sigma_2} = \frac{M_{01}}{M_{02}} \left( \frac{r_2}{r_1} \right)^3. \quad (13)$$

For example, the difference in rupture dimension between the two events of the same group that produce the variation of moment of 314 is 13 m. Considering that the largest event of the pair has a radius,  $r$  in the range 54–108 m we still obtain a relative variation of stress drop of a factor 137–213 when taking into account the size variation (see Table 1). It suggests that the variations of rupture dimension we are resolving are much too small to explain the variation of earthquake seismic moment.

## 7. Discussion

Despite different moments, colocated events seem to have very similar rupture sizes, interpreted as a large variation in stress drop.

Although we dedicated special care to ensure that the earthquake spectra analysis yields information on the event source properties, it is still possible that attenuation or path effects are affecting our results causing a bias in our estimations of rupture size and relative rupture sizes. Because of the limited bandwidth we used, a possible scenario to explain our data could be that both the largest event and the smallest event of each group have a very large corner frequency, beyond the frequency range we are currently resolving. However, this scenario is unlikely for two reasons. First, we do not observe a decay of the spectral ratio up to the highest possible frequency at the closest station (FOR) (the less affected by attenuation) (Figure 7, bottom). It would then require that the largest event has an unusually high, beyond 75 Hz, corner frequency. Second, when compared to the spectra of closely small earthquakes, the spectrum of the large event of group 4 show a distinct spectral shape after the 10–20 Hz frequency range with a more pronounced decay (Figure 8). It suggests that the corner frequency of this event is located within this 10–20 Hz frequency range and also that we can detect possible variations of corner frequencies.

Our preferred interpretation of the earthquake stress drop assumes that there is no variation of the rupture dimension between the events of the same group. Although we resolve some variations of rupture dimension, these variations are small, of the same order of magnitude as the attached uncertainties, and remain small in comparison to the dimension of the seismic rupture. In our computation of rupture dimensions, and the difference in rupture dimensions, from spectral analysis, we always assumed that the earthquake rupture velocity is constant and does not change from one event to the other within the same group. As the rupture duration has to remain fixed for all events of the same group in order to produce the same recorded waveform, it would be a possible scenario to let the earthquake size vary from one event to the other and to balance this variation by a change of rupture speed. However, although earthquake rupture velocity has been observed to vary for earthquakes in nature, this value remains generally limited in a narrow range, typically  $0.7\text{--}0.9 \beta$  [Kanamori and Brodsky, 2004]. It is then difficult to explain the large variation of moment observed in our cases as a variation of rupture velocity. Indeed, keeping a constant stress drop between the two events that exhibit a factor of nearly 300 of amplitude difference would require a change of rupture velocity by a factor  $\sqrt[3]{300} = 7$ , much larger than the observed range of rupture velocity for most earthquakes.

We look at each of the four identified groups to observe if stress drop varies in a coherent manner with time or exhibit any clear trend that would reveal a progressive mechanism at play during the circulation experiment, or at least during the lifetime of the earthquake group. However, we do not resolve any clear pattern emerging when looking at this variation of stress drop with time. We also do not observe any clustering of the large stress drop or low stress drop events at a particular time during the circulation experiment when the four groups are all analyzed together. We rather observe several rapid fluctuations in the stress drop for earthquakes of the same group. Notably, we identify a variation of a factor about 40 between two events of group 2 (event 7 and 8) in about 4 h. The two events occurred on 25 February 2010 at 00:18 and 04:37 and have reported magnitude in the catalog  $M_D$  2.1 and 0.5. This suggests that the stress drop variations are caused by a local short-term variation at the multiplet location rather than by a global process taking place over long timescale.

A viable hypothesis that would explain the resolved relative variation of moment would be to consider a change in the shear modulus,  $\mu$ , with time. This change could result from the progressive perturbation of the reservoir by fluid circulation, by the development of the induced seismicity and by a change of temperature. However, this circulation experiment remains a small perturbation to the medium when compared to fluid injection that resulted in more than 11,000 seismic events [e.g., Cuenot *et al.*, 2008]. Even in this last case, the inferred velocity changes remained small and on the order of a few percent [Calò *et al.*, 2011]. Following Spencer and Nur [1976], we quantified the effect of temperature fluctuations on the shear modulus. Considering a temperature reduction in a reservoir as large as  $50^\circ\text{C}$ , it would induce a change of the shear modulus for the rock at Soultz of only 0.3%. Similarly we do not resolve large variations of the  $S$  wave speed with the time of the circulation that would manifest as a progressive increase in the residuals of the  $S$  wave picks during the location process.

We can also estimate the possible effect of a change of attenuation,  $Q_p$ , as a way to explain the variation of waveform amplitude. Following Rubino *et al.* [2013] the expected change of waveform amplitude at 10 Hz due to the increase of the reservoir connectivity would be of the order of 12%. In our case, this is much too small to account for the observed variations. A change in attenuation resulting from a change of temperature is more difficult to quantify and would certainly be also negligible as the considered temperatures are very far from the melting point of the host rocks [Jackson and Anderson, 1970]. Finally, because we are also observing rapid fluctuations (increasing or decreasing) of the moment in a given group, it suggests that the mechanism responsible for these fluctuations can act quickly and in a reversible way. All these factors suggest that the variation of moment is certainly not related to a change of  $\mu$  or  $Q_p$  but is more likely linked to a variation of seismic slip and static stress drop.

Similar observations of moment variation, but with smaller amplitude, for events with a constant corner frequency were also reported by Bourouis and Bernard [2007] during the 1993 stimulation at Soultz. Analysis of induced earthquakes in other geothermal fields also showed local fluctuations of the stress drop related to a change of fluid pressure caused by injection [Pearson, 1981; Goertz-Allmann *et al.*, 2011; Chen and Shearer, 2011]. The same observations were also made recently for events recorded in Taiwan along the Chelungpu fault [Lin *et al.*, 2013]. Here we show that the identified variations are occurring at the same location and,

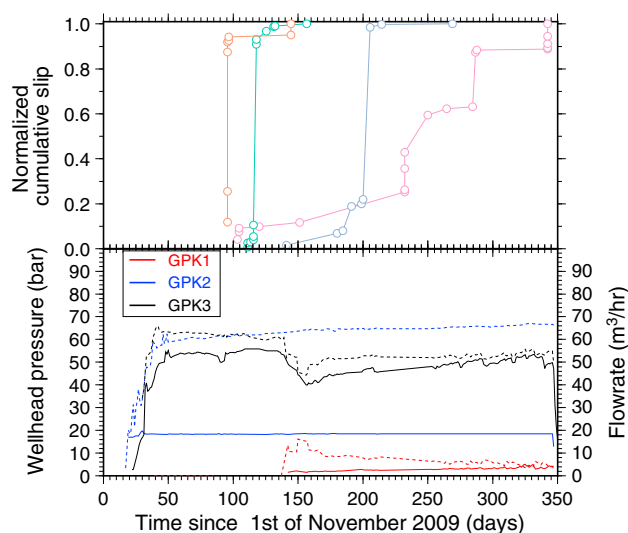


**Figure 9.** (top) Evolution with time of the seismic slip inferred for the four identified repeating event sequences. Each color represents a different sequence as in the previous figures. The slip of each event in a given sequence is normalized by the final cumulative slip of the sequence. (bottom) Evolution of the hydraulic parameters during the circulation experiments. Flow rates are given by the dashed lines and wellhead pressure by the plain lines. The colors refer to the three wells used during the circulation.

as such we can attribute these variations uniquely to a change of the environmental conditions that can vary quickly within the reservoir. The most likely candidate affecting the stress drop of the events is the fluid pressure acting on the interface of each asperity.

Local fluid pressure fluctuations are expected during the circulation experiment due to the injection of water in the reservoir. Although we do not observe a clear correlation between the hydraulic parameters (flow rate and wellhead pressure of each borehole) recorded at the surface, which are quasi-constant during circulation test (Figure 9), it is likely that the fluid pressure fluctuates locally within the reservoir. This is caused by the strong channeling [e.g., *Neuville et al.*, 2010] of new pathways for fluid circulation created by earthquakes and slow slip on various interfaces of the reservoir. It might then lead locally to a rapid increase of the fluid pressure. Furthermore, as fluid might be trapped on the shear failure interface, slip on the inter-

face will cause variations of the fluid pressure because the roughness of the fault plane will change the volume available for fluid when slipping [e.g., *Pine and Batchelor*, 1984]. This increase of fluid pressure results in a local decrease of the effective normal stress,  $\sigma'$ , defined as  $\sigma' = \sigma_n - P_f$ , where  $P_f$  is the fluid pressure and  $\sigma_n$  is the normal stress. Such a decrease in effective normal stress could then be responsible for the low values of stress drop we are observing. Indeed, considering that the largest magnitude event of each group have a typical stress drop of 3 MPa which would be compatible with their estimated rupture size, it yields a stress drop of  $\sim 3 \text{ MPa}/300 = 10 \text{ kPa}$  for the smallest resolvable events. A reduced effective normal stress has also been proposed to explain the low values of stress drop for very low frequency events observed in Japan [*Ito and Obara*, 2006]. It could be possible that lower amplitude events with even lower stress drop are occurring on the same asperities as the one identified, but we fail to detect these events as they would only emerge slightly from background noise. Resolving the existence of such smaller events would require a dedicated instrumentation with borehole sensors which unfortunately were not available during the course of this circulation test.

We can make the hypothesis that low stress drop events are related to the occurrences of aseismic slip in the reservoir. As normal stress is reduced on the fault plane, the friction mechanics on the interface will tend to produce stable slip movement [e.g., *Scholz*, 2002]. It is thus readily possible that close to the asperity where repeating earthquakes nucleate, lower strength material affected by the reduced normal stress is slipping slowly. It is also possible that on the asperity itself, the low normal stress produces more aseismic slip during the nucleation phase and after the dynamic rupture. It would then be possible to have completely aseismic events on these asperities if the effective normal stress becomes so low that no instability can nucleate on the interface [*Dieterich*, 1992]. In the context of friction mechanics and friction laws, geothermal reservoirs are a good candidate for hosting aseismic motions. They are at a shallow depth where temperature and normal stress combine to favor stable slip [*Scholz*, 1998]. This is supported by the numerous observations of aseismic slips in geothermal reservoirs and in the Soultz reservoir in particular [*Cornet et al.*, 1997; *Bourouis and Bernard*, 2007; *Calò et al.*, 2011]. This suggests that the small seismic slip events we are resolving might be related to some larger aseismic transients within the reservoir. The injection of water in the geothermal reservoir can be considered as acting in two ways: first, it promotes failures and earthquakes as the reduction in effective normal stress brings the fault planes of the reservoir closer to the Mohr envelope. Second,

and at the same time, the reduction of normal stress acts at stabilizing the slip on the interface with more displacement taking part aseismically.

Finally, an alternative hypothesis to relate these low stress drop events to aseismic motions will be to consider change of temperature induced by the circulation of the fluid within the reservoir. As temperature will fluctuate with the fluid pathway it could also provide a means to change the local condition on the interface and notably its frictional stability. It is, however, difficult to assess the variation of temperature locally on the interfaces hosting these repeating earthquakes.

## 8. Conclusion

By analyzing repeating earthquakes that occur during a circulation experiment in the Soultz-sous-Forêts geothermal reservoir, we find that events within a repeating, collocated group, have similar rupture sizes and similar locations, despite varying catalog magnitude. However, we also show that they can exhibit large fluctuations in amplitude that can be related to fluctuations of moment, stress drop, or seismic slip. We show that some events show very low seismic slip, producing a seismic signal barely emerging from the background noise. We interpret these signals as the result of a reduced effective normal stress on the interface caused by the increased fluid pressure. This low normal stress is also interpreted as responsible for the numerous aseismic motions observed in the geothermal reservoir. Our results document how normal stress variations affect the seismic behavior of an interface. Our study suggests that the increase of fluid pressure during water injection can act in two ways: it promotes failure as the state of stress on the fault plane reaches the Mohr envelope while, at the same time, it also stabilizes slip and produces aseismic motions.

### Acknowledgements

We thank Michel Bouchon, Francois Cornet, Zacharie Duputel, and Maximilien Lehujeur for discussions, and Michael Heap for grammatical assistance. Figures were made with the GMT software [Wessel and Smith, 1998]. We thank A. Baltay and an anonymous reviewer for useful comments. This work has been published under the framework of the LABEX ANR-11-LABX-0050\_G-EAU-THERMIE-PROFONDE and benefits from a funding from the state managed by the French National Research Agency as part of the Investments for the future program.

### References

- Abercrombie, R. E. (1995), Earthquake source scaling relationships from  $-1$  to 5 ML using seismograms recorded at 2.5-km depth, *J. Geophys. Res.*, *100*(B12), 24,015–24,036.
- Allmann, B. P., and P. M. Shearer (2009), Global variations of stress drop for moderate to large earthquakes, *J. Geophys. Res.*, *114*, B01310, doi:10.1029/2008JB005821.
- Baltay, A., G. Prieto, and G. C. Beroza (2010), Radiated seismic energy from coda measurements and no scaling in apparent stress with seismic moment, *J. Geophys. Res.*, *115*, B08314, doi:10.1029/2009JB006736.
- Baltay, A., S. Ide, G. Prieto, and G. Beroza (2011), Variability in earthquake stress drop and apparent stress, *Geophys. Res. Lett.*, *38*, L06303, doi:10.1029/2011GL046698.
- Ben-Zion, Y. (2008), Collective behavior of earthquakes and faults: Continuum-discrete transitions, progressive evolutionary changes, and different dynamic regimes, *Rev. Geophys.*, *46*, RG4006, doi:10.1029/2008RG000260.
- Bourouis, S., and P. Bernard (2007), Evidence for coupled seismic and aseismic fault slip during water injection in the geothermal site of Soultz (France), and implications for seismogenic transients, *Geophys. J. Int.*, *169*(2), 723–732.
- Brodsky, E. E., and J. Mori (2007), Creep events slip less than ordinary earthquakes, *Geophys. Res. Lett.*, *34*, L16309, doi:10.1029/2007GL030917.
- Brown, J. R., G. C. Beroza, S. Ide, K. Ohta, D. R. Shelly, S. Y. Schwartz, W. Rabbel, M. Thorwart, and H. Kao (2009), Deep low-frequency earthquakes in tremor localize to the plate interface in multiple subduction zones, *Geophys. Res. Lett.*, *36*, L19306, doi:10.1029/2009GL040027.
- Brune, J. N. (1970), Tectonic stress and the spectra of seismic shear waves from earthquakes, *J. Geophys. Res.*, *75*(26), 4997–5009.
- Calò, M., C. Dorbath, F. Cornet, and N. Cuenot (2011), Large-scale aseismic motion identified through 4-DP-wave tomography, *Geophys. J. Int.*, *186*(3), 1295–1314.
- Candela, T., F. Renard, M. Bouchon, J. Schmittbuhl, and E. E. Brodsky (2011), Stress drop during earthquakes: Effect of fault roughness scaling, *Bull. Seismol. Soc. Am.*, *101*(5), 2369–2387.
- Charl y, J., N. Cuenot, L. Dorbath, C. Dorbath, H. Haessler, and M. Frogneux (2007), Large earthquakes during hydraulic stimulations at the geothermal site of Soultz-sous-For ts, *Int. J. Rock Mech. Min.*, *44*(8), 1091–1105.
- Chen, X., and P. Shearer (2011), Comprehensive analysis of earthquake source spectra and swarms in the Salton Trough, California, *J. Geophys. Res.*, *116*, B09309, doi:10.1029/2011JB008263.
- Cornet, F., J. Helm, H. Poitrenaud, and A. Etchecopar (1997), Seismic and aseismic slips induced by large-scale fluid injections, *Pure Appl. Geophys.*, *150*, 563–583.
- Cuenot, N., C. Dorbath, and L. Dorbath (2008), Analysis of the microseismicity induced by fluid injections at the EGS site of Soultz-sous-For ts (Alsace, France): Implications for the characterization of the geothermal reservoir properties, *Pure Appl. Geophys.*, *165*(5), 797–828.
- Cuenot, N., M. Frogneux, C. Dorbath, and M. Calo (2011), Induced microseismic activity during recent circulation tests at the EGS site of Soultz-sous-For ts (France), paper presented at Thirty-Sixth Workshop on Geothermal Reservoir Engineering, Stanford Univ., Stanford, Calif., 31 Jan.–2 Feb.
- Dieterich, J. H. (1992), Earthquake nucleation on faults with rate- and state-dependent strength, *Tectonophysics*, *211*(1–4), 115–134.
- Dorbath, L., N. Cuenot, A. Genter, and M. Frogneux (2009), Seismic response of the fractured and faulted granite of soultz-sous-for ts (France) to 5 km deep massive water injections, *Geophys. J. Int.*, *177*(2), 653–675.
- Duputel, Z., V. C. Tsai, L. Rivera, and H. Kanamori (2013), Using centroid time-delays to characterize source durations and identify earthquakes with unique characteristics, *Earth Planet. Sci. Lett.*, *374*, 92–100.
- Eshelby, J. D. (1957), The determination of the elastic field of an ellipsoidal inclusion, and related problems, *Proc. R. Soc. London, Ser. A*, *241*(1226), 376–396.

- Goertz-Allmann, B. P., A. Goertz, and S. Wiemer (2011), Stress drop variations of induced earthquakes at the Basel geothermal site, *Geophys. Res. Lett.*, *38*, L09308, doi:10.1029/2011GL047498.
- Got, J.-L., and J. Fréchet (1993), Origins of amplitude variations in seismic doublets: Source or attenuation process?, *Geophys. J. Int.*, *114*(2), 325–340.
- Got, J.-L., and P. Okubo (2003), New insights into Kilauea's volcano dynamics brought by large-scale relative relocation of microearthquakes, *J. Geophys. Res.*, *108*(B7), 2237, doi:10.1029/2002JB002060.
- Got, J.-L., J. Fréchet, and F. W. Klein (1994), Deep fault plane geometry inferred from multiplet relative relocation beneath the south flank of Kilauea, *J. Geophys. Res.*, *99*(B8), 15,375–15,386.
- Got, J.-L., V. Monteiller, J. Guilbert, D. Marsan, Y. Cansi, C. Maillard, and J.-P. Santoire (2011), Strain localization and fluid migration from earthquake relocation and seismicity analysis in the western Vosges (France), *Geophys. J. Int.*, *185*(1), 365–384.
- Harrington, R. M., and E. E. Brodsky (2009), Source duration scales with magnitude differently for earthquakes on the San Andreas Fault and on secondary faults in Parkfield, California, *Bull. Seismol. Soc. Am.*, *99*(4), 2323–2334.
- Hooijkaas, G. R., A. Genter, and C. Dezayes (2006), Deep-seated geology of the granite intrusions at the Soultz EGS site based on data from 5km-deep boreholes, *Geothermics*, *35*(5), 484–506.
- Hough, S. (1997), Empirical Green's function analysis: Taking the next step, *J. Geophys. Res.*, *102*(B3), 5369–5384.
- Ito, Y., and K. Obara (2006), Very low frequency earthquakes within accretionary prisms are very low stress-drop earthquakes, *Geophys. Res. Lett.*, *33*, L09302, doi:10.1029/2006GL025883.
- Jackson, D. D., and D. L. Anderson (1970), Physical mechanisms of seismic-wave attenuation, *Rev. Geophys.*, *8*(1), 1–63.
- Kanamori, H. (1977), The energy release in great earthquakes, *J. Geophys. Res.*, *82*(20), 2981–2987.
- Kanamori, H. (2004), The diversity of the physics of earthquakes, *Proc. Jpn. Acad. Ser. B*, *80*, 297–316.
- Kanamori, H., and E. E. Brodsky (2004), The physics of earthquakes, *Rep. Prog. Phys.*, *67*(8), 1429–1496, doi:10.1088/0034-4885/67/8/R03.
- Kane, D. L., G. A. Prieto, F. L. Vernon, and P. M. Shearer (2011), Quantifying seismic source parameter uncertainties, *Bull. Seismol. Soc. Am.*, *101*(2), 535–543.
- Kaneko, Y., J.-P. Ampuero, and N. Lapusta (2011), Spectral-element simulations of long-term fault slip: Effect of low-rigidity layers on earthquake-cycle dynamics, *J. Geophys. Res.*, *116*, B10313, doi:10.1029/2011JB008395.
- Klein, F. W., (2002), User's guide to hypoinverse-2000: A fortran program to solve for earthquake locations and magnitudes, *U.S. Geol. Surv. Open File Rep.*, U. S. Geological Survey, Menlo Park, Calif.
- Latour, S., T. Gallot, S. Catheline, C. Voisin, F. Renard, E. Larose, and M. Campillo (2011), Ultrafast ultrasonic imaging of dynamic sliding friction in soft solids: The slow slip and the super-shear regimes, *Europhys. Lett.*, *96*(5), 59003, doi:10.1209/0295-5075/96/59003.
- Lengliné, O., and J.-L. Got (2011), Rupture directivity of microearthquake sequences near Parkfield, California, *Geophys. Res. Lett.*, *38*, L08310, doi:10.1029/2011GL047303.
- Lin, Y.-Y., T.-R. A. Song, and K.-F. Ma (2013), Investigating source scaling of earthquake clusters using the TCDP borehole seismometers in Taiwan, Abstract T51D-2501 presented at 2013 Fall Meeting, AGU, San Francisco, Calif., [Available at <http://abstractsearch.agu.org/meetings/2013/FM/sections/T/sessions/T51D/abstracts/T51D-2501.html>].
- Lockner, D. A., P. G. Okubo, and J. H. Dieterich (1982), Containment of stick-slip failures on a simulated fault by pore fluid injection, *Geophys. Res. Lett.*, *9*(8), 801–804.
- Madariaga, R. (1977), High-frequency radiation from crack (stress drop) models of earthquake faulting, *Geophys. J. R. Astron. Soc.*, *51*(3), 625–651.
- Malagnini, L., S. Nielsen, K. Mayeda, and E. Boschi (2010), Energy radiation from intermediate-to large-magnitude earthquakes: Implications for dynamic fault weakening, *J. Geophys. Res.*, *115*, B06319, doi:10.1029/2009JB006786.
- Mayeda, K., and W. R. Walter (1996), Moment, energy, stress drop, and source spectra of western United States earthquakes from regional coda envelopes, *J. Geophys. Res.*, *101*(B5), 11,195–11,208.
- Mayeda, K., L. Malagnini, and W. R. Walter (2007), A new spectral ratio method using narrow band coda envelopes: Evidence for non-self-similarity in the Hector Mine sequence, *Geophys. Res. Lett.*, *34*, L11303, doi:10.1029/2007GL030041.
- Meng, L., A. Inbal, and J.-P. Ampuero (2011), A window into the complexity of the dynamic rupture of the 2011 Mw 9 Tohoku-Oki earthquake, *Geophys. Res. Lett.*, *38*, L00G07, doi:10.1029/2011GL048118.
- Neuville, A., R. Toussaint, and J. Schmittbuhl (2010), Hydrothermal coupling in a self-affine rough fracture, *Phys. Rev. E*, *82*(3), 36317, doi:10.1103/PhysRevE.82.036317.
- Ougier-Simonin, A., and W. Zhu (2013), Effects of pore fluid pressure on slip behaviors: An experimental study, *Geophys. Res. Lett.*, *40*, 2619–2624, doi:10.1002/grl.50543.
- Pearson, C. (1981), The relationship between microseismicity and high pore pressures during hydraulic stimulation experiments in low permeability granitic rocks, *J. Geophys. Res.*, *86*(B9), 7855–7864.
- Peng, Z., and J. Gombert (2010), An integrated perspective of the continuum between earthquakes and slow-slip phenomena, *Nat. Geosci.*, *3*(9), 599–607.
- Pine, R., and A. Batchelor (1984), Downward migration of shearing in jointed rock during hydraulic injections, *Int. J. Rock Mech. Min. Sci.*, *21*(5), 249–263.
- Rubino, J., L. Guarracino, T. M. Müller, and K. Holliger (2013), Do seismic waves sense fracture connectivity?, *Geophys. Res. Lett.*, *40*, 692–696, doi:10.1002/grl.50127.
- Rubinstein, J. L., and W. L. Ellsworth (2010), Precise estimation of repeating earthquake moment: Example from Parkfield, California, *Bull. Seismol. Soc. Am.*, *100*(5A), 1952–1961.
- Sausse, J., C. Dezayes, L. Dorbath, A. Genter, and J. Place (2010), 3d model of fracture zones at Soultz-sous-Forêts based on geological data, image logs, induced microseismicity and vertical seismic profiles, *C. R. Geosci.*, *342*(7), 531–545.
- Scholz, C. H. (1998), Earthquakes and friction laws, *Nature*, *391*(6662), 37–42.
- Scholz, C. H. (2002), *The Mechanics of Earthquakes and Faulting*, Cambridge Univ. Press, Cambridge, U. K.
- Spencer, J. W., and A. M. Nur (1976), The effects of pressure, temperature, and pore water on velocities in westerly granite, *J. Geophys. Res.*, *81*(5), 899–904.
- Wessel, P., and W. H. Smith (1998), New, improved version of generic mapping tools released, *Eos Trans. AGU*, *79*(47), 579–579.
- Wiens, D. A. (2001), Seismological constraints on the mechanism of deep earthquakes: Temperature dependence of deep earthquake source properties, *Phys. Earth Planet. Inter.*, *127*(1), 145–163.